

# GigaScience

## Integrating deep mutational scanning and lowthroughput mutagenesis data to predict the impact of amino acid variants

--Manuscript Draft--

<b>Manuscript Number:</b>	GIGA-D-23-00040	
<b>Full Title:</b>	Integrating deep mutational scanning and lowthroughput mutagenesis data to predict the impact of amino acid variants	
<b>Article Type:</b>	Research	
<b>Funding Information:</b>	Melbourne Research Scholarship	Mr Yunfan Fu
	National Health and Medical Research Council (116955)	Professor Anthony Troy Papenfuss
	Lorenzo and Pamela Galli Medical Research Trust	Professor Anthony Troy Papenfuss
	Stafford Fox Medical Research Foundation	Professor Anthony Troy Papenfuss
	National Human Genome Research Institute (RM1HG010461)	Dr Alan F. Rubin
	National Human Genome Research Institute (UM1HG011969)	Dr Alan F. Rubin
<b>Abstract:</b>	<p>Background: Evaluating the impact of amino acid variants has been a critical challenge for studying protein function and interpreting genomic data. High-throughput experimental methods like deep mutational scanning (DMS) can measure the effect of large numbers of variants in a target protein, but because DMS studies have not been performed on all proteins, researchers also model DMS data computationally to estimate variant impacts by predictors.</p> <p>Results: In this study, we extended a linear regression-based predictor to explore whether incorporating data from alanine scanning (AS), a widely-used low-throughput mutagenesis method, would improve prediction results. To evaluate our model, we collected 146 AS datasets, mapping to 54 DMS datasets across 22 distinct proteins.</p> <p>Conclusions: We show that improved model performance depends on the compatibility of the DMS and AS assays, and the scale of improvement is closely related to the correlation between DMS and AS results.</p>	
<b>Corresponding Author:</b>	Alan F Rubin, PhD Walter and Eliza Hall Institute of Medical Research Parkville, VIC AUSTRALIA	
<b>Corresponding Author Secondary Information:</b>		
<b>Corresponding Author's Institution:</b>	Walter and Eliza Hall Institute of Medical Research	
<b>Corresponding Author's Secondary Institution:</b>		
<b>First Author:</b>	Yunfan Fu	
<b>First Author Secondary Information:</b>		
<b>Order of Authors:</b>	Yunfan Fu	
	Justin Bedó	
	Anthony Troy Papenfuss, BSc (Hons) PhD	
	Alan F. Rubin	
<b>Order of Authors Secondary Information:</b>		
<b>Additional Information:</b>		

Question	Response
<p>Are you submitting this manuscript to a special series or article collection?</p>	<p>No</p>
<p><b>Experimental design and statistics</b></p> <p>Full details of the experimental design and statistical methods used should be given in the Methods section, as detailed in our <a href="#">Minimum Standards Reporting Checklist</a>. Information essential to interpreting the data presented should be made available in the figure legends.</p> <p>Have you included all the information requested in your manuscript?</p>	<p>Yes</p>
<p><b>Resources</b></p> <p>A description of all resources used, including antibodies, cell lines, animals and software tools, with enough information to allow them to be uniquely identified, should be included in the Methods section. Authors are strongly encouraged to cite <a href="#">Research Resource Identifiers</a> (RRIDs) for antibodies, model organisms and tools, where possible.</p> <p>Have you included the information requested as detailed in our <a href="#">Minimum Standards Reporting Checklist</a>?</p>	<p>Yes</p>
<p><b>Availability of data and materials</b></p> <p>All datasets and code on which the conclusions of the paper rely must be either included in your submission or deposited in <a href="#">publicly available repositories</a> (where available and ethically appropriate), referencing such data using a unique identifier in the references and in the “Availability of Data and Materials” section of your manuscript.</p>	<p>Yes</p>

Have you have met the above requirement as detailed in our [Minimum Standards Reporting Checklist?](#)



# 1 Integrating deep mutational scanning and low- 2 throughput mutagenesis data to predict the impact of 3 amino acid variants

4

## 5 Authors:

6 Yunfan Fu<sup>1,2</sup>, Justin Bedó<sup>1,3,\*</sup>, Anthony T. Papenfuss<sup>1,2,4,\*,\*\*</sup>, Alan F. Rubin<sup>1,2,\*,\*\*</sup>

7

## 8 Affiliations:

9 <sup>1</sup>The Walter and Eliza Hall Institute of Medical Research, Parkville, 3052, Victoria, Australia.

10 <sup>2</sup>Department of Medical Biology, The University of Melbourne, Melbourne, VIC 3010, Australia.

11 <sup>3</sup>School of Computing and Information Systems, The University of Melbourne, Melbourne, VIC 3010,  
12 Australia.

13 <sup>4</sup>Peter MacCallum Cancer Centre, Melbourne, VIC 3000, Australia.

14

15 \* Contributed equally

16 \*\* To whom correspondence should be addressed ([papenfuss@wehi.edu.au](mailto:papenfuss@wehi.edu.au) &  
17 alan.rubin@wehi.edu.au)

18

## 19 Abstract

20 **Background:** Evaluating the impact of amino acid variants has been a critical challenge for  
21 studying protein function and interpreting genomic data. High-throughput experimental  
22 methods like deep mutational scanning (DMS) can measure the effect of large numbers of

23 variants in a target protein, but because DMS studies have not been performed on all proteins,  
24 researchers also model DMS data computationally to estimate variant impacts by predictors.

25 **Results:** In this study, we extended a linear regression-based predictor to explore whether  
26 incorporating data from alanine scanning (AS), a widely-used low-throughput mutagenesis  
27 method, would improve prediction results. To evaluate our model, we collected 146 AS  
28 datasets, mapping to 54 DMS datasets across 22 distinct proteins.

29 **Conclusions:** We show that improved model performance depends on the compatibility of the  
30 DMS and AS assays, and the scale of improvement is closely related to the correlation between  
31 DMS and AS results.

32

33 **Keywords:** deep mutational scanning, alanine scanning, machine learning, predictor

34

## 35 **1 Introduction**

36 Deep mutational scanning (DMS) is a functional genomics method that can experimentally  
37 measure the impact of many thousands of protein variants by combining high-throughput  
38 sequencing with a functional assay [1]. In a typical DMS, a cDNA library of genetic variants  
39 of a target gene is generated, containing all possible single amino acid substitutions. This  
40 variant library is then expressed in a functional assay system where the variants can be selected  
41 based on their properties. The change in variant frequency in the pre- and post-selection  
42 populations is determined by high-throughput sequencing which is then used to calculate a  
43 multiplexed functional score that captures the variant's impact [2–4]. The versatility of DMS  
44 assays makes it possible to measure variant impact on a wide range of protein properties,  
45 including protein binding [5,6], protein abundance [7–9], catalytic activity [10,11] and cell  
46 growth rate [12–14].

47

48 Computational studies have used DMS data to build predictive models of variant impact. These  
49 predictors use supervised or semi-supervised learning models trained on experimental DMS  
50 data and various protein features to make predictions [15–21]. Envision is one such method  
51 that used protein structural, physicochemical, and evolutionary features to predict variant effect  
52 scores and was trained on DMS data from 8 proteins using gradient boosting [15]. Another  
53 method, DeMaSk, predicted DMS scores by combining two evolutionary features (protein  
54 positional conservation and variant homologous frequency) with a DMS substitution matrix  
55 and was trained on data from 17 proteins using a linear model [17]. Deep learning algorithms  
56 have also been applied to build protein fitness predictors [16,18], which are usually based only  
57 on variant sequences.

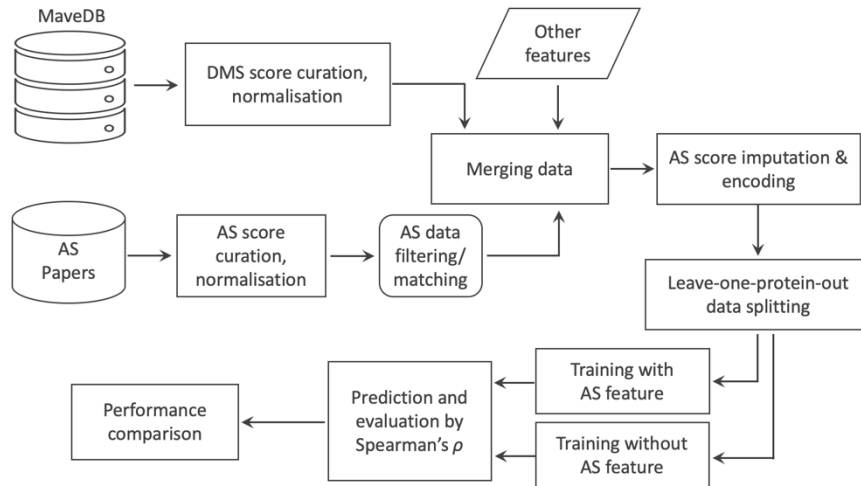
58

59 Low-throughput mutagenesis experiments that measure tens of variants at a time have also  
60 been used extensively to study diverse protein properties, including substrate binding affinity  
61 [22,23], protein stability [24,25], and protein activity [26,27]. Alanine scanning (AS) is a  
62 widely-used low-throughput mutagenesis method [28,29], and AS data are available for many  
63 proteins. In this method, each targeted protein residue is substituted with alanine, and the  
64 impacts of these variants are measured by a functional assay [30]. AS experiments are typically  
65 used to identify functional hot spots or critical residues in the target protein [31,32] and have  
66 been used as a source of independent validation for DMS studies [27,33–35].

67

68 In this study, we explore whether a predictive model can be improved by incorporating low-  
69 throughput mutagenesis data (Fig 1). We find that AS data can increase prediction accuracy  
70 and that the improvement is related to the similarity of the functional assays and the correlation  
71 of DMS and AS results.

72



73

74 **Fig 1. Workflow for model training and testing.** DMS and AS datasets are collected from online resources  
 75 and are normalized. DMS and AS datasets targeting the same protein are then matched, filtered and merged. Two  
 76 predictors are constructed and tested: the first uses DMS data, AS data and other protein features, and the second  
 77 uses only DMS data and the same other protein features.

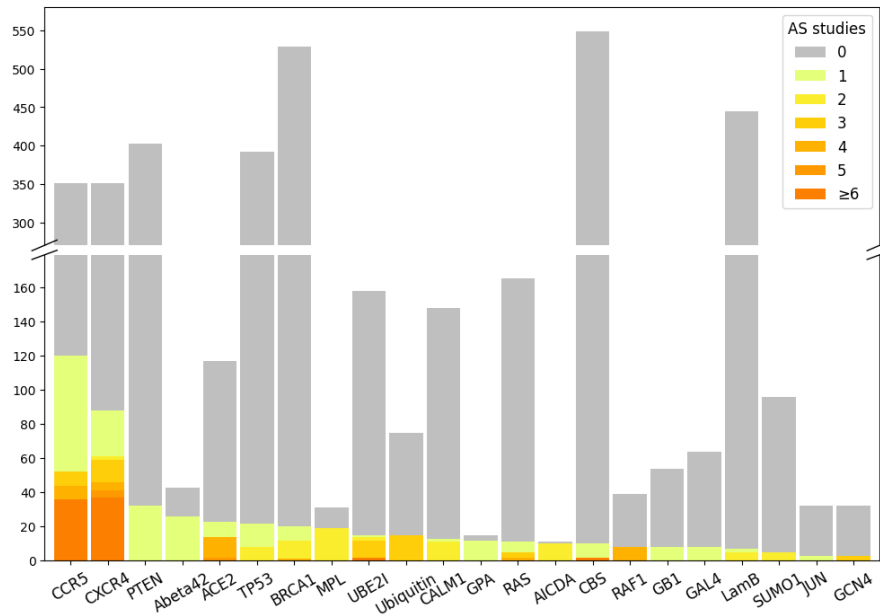
78

## 79 2 Results

### 80 2.1 Overview of DMS and alanine scanning (AS) data

81 To build the predictive model, 130 DMS datasets were collected from MaveDB [36,37]  
 82 (Supplementary table 1). We searched the literature and found 146 AS datasets targeting the  
 83 same proteins as 54 of the DMS datasets. In total, we obtained both DMS and AS data for 22  
 84 different proteins: 17 human proteins, three yeast proteins, and two bacterial proteins. Most  
 85 DMS experiments were highly complete, with a mean coverage of 95.0% of all possible single  
 86 amino acid substitutions assayed in the target region, comprising 373,219 total protein variant  
 87 measurements. AS data were only available on a small number of protein residues (Fig 2), and  
 88 we were able to curate 1,480 alanine substitution scores from the 146 studies. Variant scores  
 89 from collected DMS and AS studies were linearly normalized to a common scale (see Methods)  
 90 to make them comparable across datasets (Fig S1).

91



92

93 **Fig 2. DMS data generally cover more protein residues than AS data.** Each bar shows the number of  
 94 residues assayed by DMS studies on given target proteins. Colour indicates the number of AS studies available  
 95 for the DMS-tested residues.

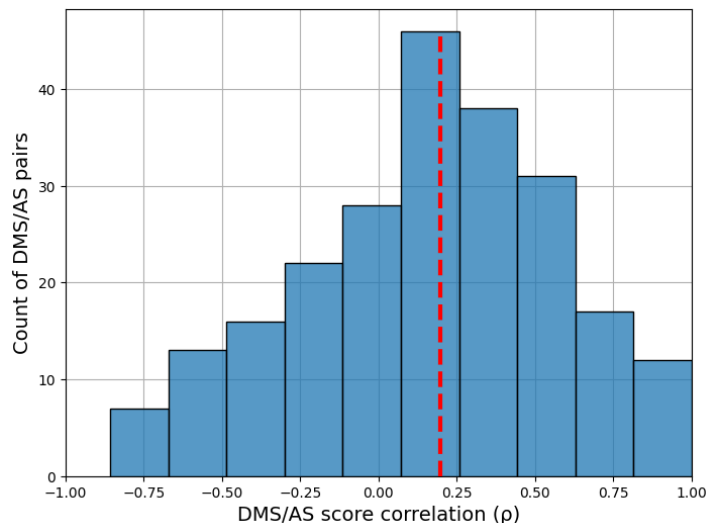
96

## 97 **2.2 The correlation of DMS and AS scores is related to assay compatibility**

98 To evaluate the similarity of AS and DMS scores, we calculated Spearman's correlation ( $\rho$ )  
 99 between the AS scores and DMS scores for the same alanine substitutions. Since each protein  
 100 may have results from several AS and DMS experiments, we calculated  $\rho$  between each  
 101 possible pair. The median  $\rho$  over DMS and AS data (DMS/AS) pairs was 0.2, indicating that  
 102 the experimental scores were poorly correlated overall (Fig 3).

103





104

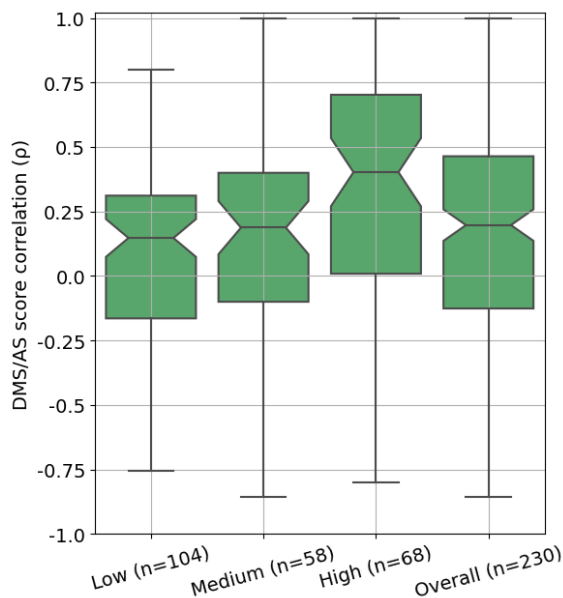
105 **Fig 3. Correlation between DMS and AS data shows substantial variation.** We calculated Spearman's  $\rho$   
 106 between alanine substitution scores in each pair of AS and DMS data. The results for pairs with less than three  
 107 alanine substitutions are removed. The red dashed line shows the median  $\rho$ .

108

109 We then considered if differences between AS and DMS assay designs might contribute to this  
 110 low agreement between scores. To explore this, we developed a decision tree (Fig S2) to  
 111 classify whether DMS/AS pairs had low, medium, or high assay compatibility, which we  
 112 defined as a similarity measurement of the functional assays performed. For example, the DMS  
 113 assay measuring the binding affinity of a cell surface protein, CXCR4, to its natural ligand [38]  
 114 has high compatibility with the AS experiment also measuring this ligand binding but has low  
 115 compatibility with the study on CXCR4's ability to facilitate virus infection [39]. A full assay  
 116 compatibility table can be found in Supplementary Table 1 with the compatibility  
 117 classifications and justification for each pair. We then compared DMS and AS score correlation  
 118 for each compatibility class and found that score correlations were closely related to assay  
 119 compatibility. Data from low compatibility assays had a median correlation of 0.15, rising to  
 120 0.19 for medium compatibility assays and 0.40 for high compatibility assays (Fig 4). This link

121 between assay compatibility and score correlation indicates that our decision tree approach was  
122 able to capture the similarity between assay systems.

123



124

125 **Fig 4. DMS and AS data pairs with high assay compatibility show a higher score correlation.** Each box  
126 represents Spearman's  $\rho$  between DMS and AS data pairs of classified assay compatibility or the overall result.  
127 The correlation coefficients are calculated between alanine substitution scores in each pair of AS and DMS data.  
128 Results for data pairs with less than three alanine substitutions are removed.

129

### 130 2.3 Compatible AS data improve DMS score prediction accuracy

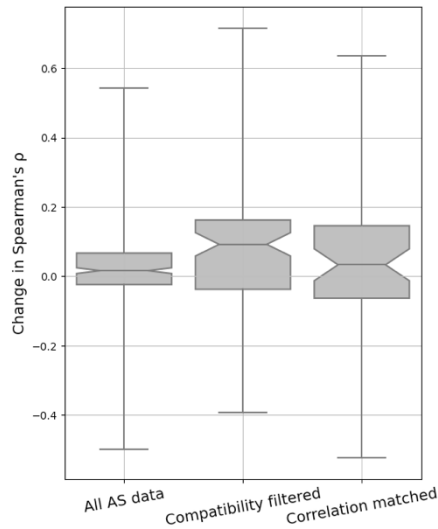
131 To test if incorporating AS data into DMS score models would improve prediction accuracy,  
132 we decided to build a new model based on DeMaSk [17]. We chose DeMaSk because it showed  
133 better performance compared to similar methods and was straightforward to modify. The  
134 published DeMaSk model predicts DMS scores using protein positional conservation, variant  
135 homologous frequency, and substitution score matrix, and we incorporated AS data as an  
136 additional feature. Our new predictor was modelled with all 130 DMS we collected and we  
137 applied a leave-one-protein-out cross-validation approach to training and testing [15].  
138 Prediction performance was evaluated using the Spearman's correlation ( $\rho$ ) between the

139 experimentally-derived DMS scores and the predicted scores for each pair of DMS and AS  
140 studies. The performance of our DMS/AS model was compared with a model trained only on  
141 DMS data, equivalent to retrained DeMaSk (Fig S3), by calculating the change of prediction  $\rho$   
142 (see Methods).

143

144 We trained our model with either all or a subset of AS data we collected (Fig 5, Table S1). We  
145 first integrated all 146 AS data collected for training and evaluation but observed only a modest  
146 improvement of prediction  $\rho$  (Fig 5 left box, and Fig S4). We then retrained and evaluated our  
147 model on filtered AS data with only high compatibility assays, and observed a median increase  
148 in prediction Spearman's  $\rho$  of 0.1 compared to the results with no AS data (Fig 5 middle box,  
149 and Fig S4). However, training with both high and medium compatibility pairs reduced the  
150 performance improvement (Fig S5). These results indicate that medium and low compatibility  
151 pairs might provide inconsistent training data, degrading model performance. We also  
152 evaluated the impact of including high compatibility AS data in an alternative model based on  
153 Envison [15], and found similar results (Fig S6). To differentiate between high assay  
154 compatibility and high DMS/AS score correlation, we trained the model using the most highly  
155 correlated AS result for each DMS dataset (see Methods). Although the upper quartile was  
156 high, the median performance change of this predictor was lower than the high assay  
157 compatibility model, suggesting that matching with the highest score correlation alone is  
158 insufficient (Fig 5 right box).

159



160

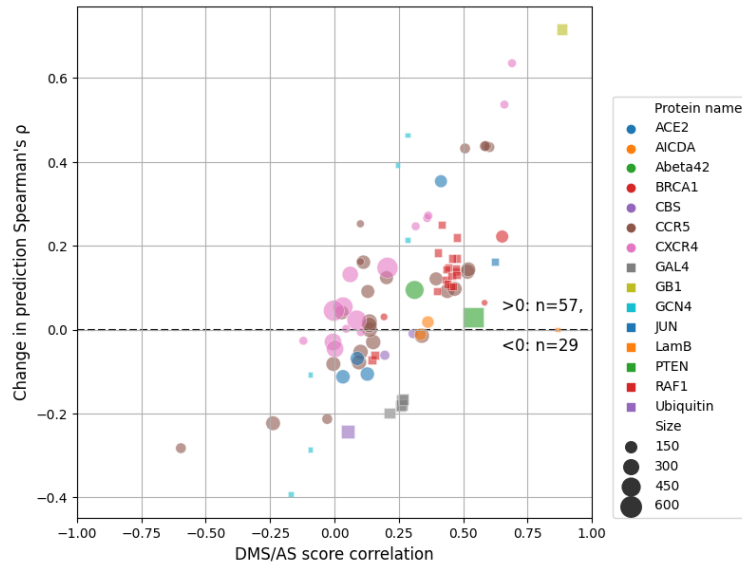
161 **Fig 5. Performance of variant impact prediction is improved using AS data with high assay compatibility.**

162 The change of prediction  $\rho$  for each DMS and AS data pair is shown as box plots. A higher value represents higher  
 163 prediction accuracy achieved for using AS data. Different approaches to filtering/matching the data are shown on  
 164 the x-axis: “All AS data” used all available data; “Compatibility filtered” used only data of high assay  
 165 compatibility; “Correlation matched” used only data with the highest regularised correlation for each DMS dataset.

166

167 To further explore the higher performance of compatibility-filtered predictor, we examined the  
 168 relationship between prediction  $\rho$  change and score correlation for each high compatibility  
 169 DMS/AS pair (Fig 6). For most pairs, prediction performance was improved by using AS data,  
 170 and the scale of improvement was also related to the score correlation. This relationship could  
 171 also be observed for multiple DMS/AS pairs from an individual protein, such as CXCR4 and  
 172 CCR5. We saw the same trend in the predictor trained with all DMS/AS pairs but noted that  
 173 the performance even of highly correlated pairs was worse, likely due to the influence of low  
 174 compatibility training data on the model (Fig S7).

175



176

177 **Fig 6. Prediction performance change is related to DMS and AS score correlation.** Each dot represents a  
 178 filtered DMS/AS data pair of high assay compatibility. The vertical axis shows the change of prediction  $\rho$  by using  
 179 AS data (larger means higher performance achieved by using AS data). The horizontal axis shows the DMS/AS  
 180 score correlation for *all* variants on the matched residues rather than just alanine substitutions. The colours and  
 181 shapes of the dots correspond to the target protein, and size indicates the number of variants in each data pair.

182

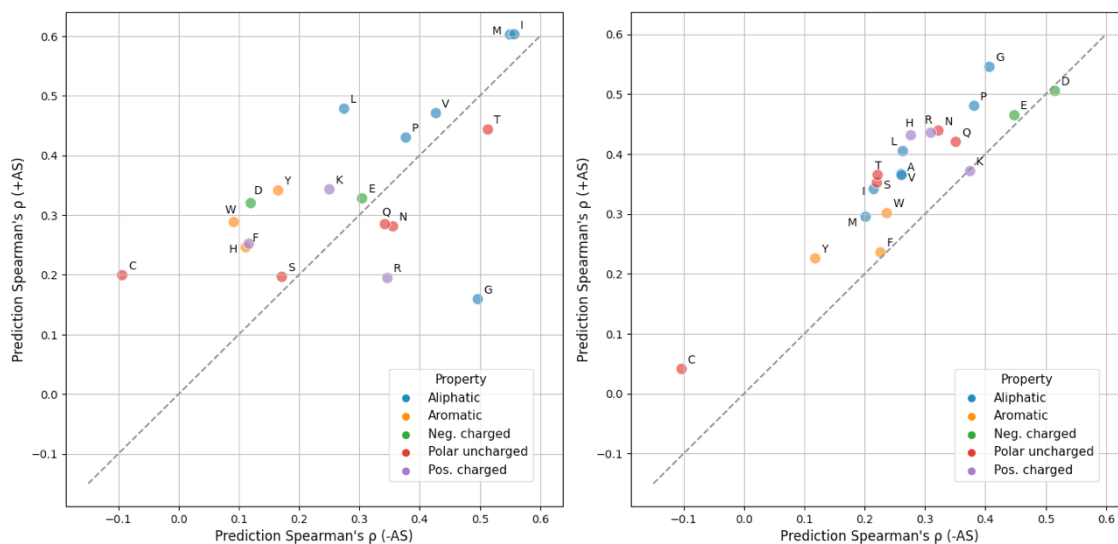
183 We also explored the consequences of the sparsity of AS data on our model in two ways: by  
 184 using a boosting approach that focuses only on residues with AS data (Fig S8) and by using  
 185 complete alanine substitution information from DMS as the AS feature (Fig S9). Both of these  
 186 approaches performed very similarly to the primary model constructed using high-  
 187 compatibility DMS/AS data and simple mean score imputation.

188

189 To test the influence of amino acids on our predictor, we grouped the prediction results by  
 190 either wild-type or variant amino acid and calculated the prediction improvement when AS  
 191 data were included (Fig 7). We found that 14 of 19 wild-type amino acids performed better  
 192 with the addition of AS data, with cysteine showing the largest improvement and performing  
 193 worst in the model lacking AS data. 18 of 20 variant amino acids benefited from the inclusion

194 of AS data, with marginal performance decrease on lysine and aspartic acid ( $|\Delta\rho|<0.01$ ) (Fig  
195 7).

196



197

198 **Fig 7. Model performance is generally improved for each wild-type and variant amino acid.** Prediction

199 Spearman's  $\rho$  when using (y-axis) or not using (x-axis) AS data on each wild-type (left) or variant (right) amino  
200 acid is shown in the scatter plots. The results are coloured according to the property of each amino acid type.

201 Alanine (A) result is not applicable in the first figure since alanine scanning data are always missing when the

202 wildtype is alanine itself. Absolute count for each amino acid can be found in Fig S10. (Neg.: negatively, Pos.:

203 positively)

204

### 205 3 Discussion

206 In this study, we integrated alanine scanning (AS) data into deep mutational scanning (DMS)

207 score prediction, leading to modest improvements in the accuracy of variant score prediction.

208 We also explored the impact of the diversity of protein properties measured by DMS and AS.

209 Filtering DMS and AS data based on our manual classification of assay type compatibility led

210 to improved prediction performance.

211

212 A potential shortcoming of our current approach is that AS data were available for only a small  
213 proportion of the DMS data. Although most recent DMS studies can analyze variants of the  
214 whole protein, most AS experiments only cover a handful of residues in the target protein,  
215 leaving missing AS scores for the vast majority of residues. We explored this here and found  
216 that alternative methods for addressing the sparsity of AS data did not improve or degrade  
217 performance, but we anticipate further improved prediction accuracy if the low completeness  
218 and unevenness of AS data are appropriately handled before modelling, such as by advanced  
219 imputation methods [48,49].

220

221 In this study, we identified the importance of DMS/AS assay compatibility as a crucial factor  
222 for improving prediction accuracy. An issue with using this concept is that it further shrinks  
223 already sparse data. It also fails to take advantage of the fact that even for low compatible  
224 assays some fundamental information like protein stability can still be mutually captured.  
225 Instead of hard filtering, proper implementation of this underlying information may facilitate  
226 variant impact prediction in the future. Nonetheless, filtering on assay compatibility still leads  
227 to performance improvement. We also briefly explored whether the consistency of DMS and  
228 AS scores can be considered more directly by matching the best correlated AS data for each  
229 DMS dataset. Consistency is partially driven by assay compatibility but also reflects other  
230 features of the data, such as bias and noise. While we picked the most correlated pair for each  
231 DMS, we did not threshold the correlation, potentially including data pairs that were poor  
232 matches.

233

234 The concepts of compatibility and data quality are also relevant to training any DMS-based  
235 predictors. DMS assays have been developed to measure variant impacts to distinct protein  
236 properties, and a variant can behave similarly to wildtype when measured by one assay yet

237 show altered protein properties in other assay results, which are frequently found in regions  
238 with specific biochemical functions [50–55]. With more experimental assays to be applied, the  
239 diverse measurements may impede the progress of future DMS-based predictors unless this  
240 assay effect is properly addressed, for example, by building assay specific predictors.  
241 Measurement error is another source of DMS data heterogeneity that potentially affects the  
242 model performance. In our current study, DMS scores of protein variants are weighted equally  
243 while training. Adjustable weighting can be applied in future studies to adapt the distinct  
244 experimental error between individual variants and datasets, reducing the influence of low-  
245 confident data.

246

247 In summary, we conclude that the careful inclusion of low-throughput mutagenesis data  
248 improves the prediction of DMS scores, and the approaches described here can potentially be  
249 applied to other prediction methods.

250

#### 251 **4 Availability of supporting source code and requirements**

252 **Project name:** DMS\_with\_Alanine\_scan

253 **Project home page:** [https://github.com/PapenfussLab/DMS\\_with\\_Alanine\\_scan](https://github.com/PapenfussLab/DMS_with_Alanine_scan)

254 **Operating system:** Platform independent

255 **Programming language:** Python

256 **Other requirements:** Python 3.10.6

257 **Licence:** MIT Licence

258

#### 259 **5 List of abbreviations**

260 DMS: deep mutational scanning

261 AS: alanine scanning



262

## 263 **6 Supporting information**

264 **Supplementary Table 1:** All candidate DMS and alanine scanning data with detailed dataset  
265 information.

266 **Supplementary Table 2:** Normalized DMS dataset with protein property features.

267 **Supplementary Table 3:** Normalized alanine scanning dataset.

268

## 269 **7 Author contributions**

270 YF developed the software and wrote the initial draft of the manuscript. AFR conceived the  
271 study. JB, AFR, and ATP oversaw the project. All authors reviewed, contributed to, and  
272 approved the manuscript.

273

## 274 **8 Funding**

275 YF is supported by Melbourne Research Scholarship. ATP was supported by an  
276 Australian National Health and Medical Research Council (NHMRC) Senior Research  
277 Fellowship (1116955). JB, AFR and ATP were supported by the Lorenzo and Pamela Galli  
278 Medical Research Trust. JB and ATP were supported by the Stafford Fox Medical Research  
279 Foundation. AFR was supported by the National Human Genome Research Institute of the NIH  
280 under award numbers RM1HG010461 and UM1HG011969. The research benefitted from  
281 support from the Victorian State Government Operational Infrastructure Support and  
282 Australian Government NHMRC Independent Research Institute Infrastructure Support.

283

## 284 **9 Methods**

### 285 **9.1 DMS data collection**

286 DMS data were downloaded from MaveDB [36,37] which were then filtered and curated. DMS  
287 experiments targeting antibody and virus proteins were removed because of their potentially  
288 unique functionality. We retrieved the UniProt accession ID of target proteins by searching the  
289 protein names or sequences in UniProt [56], and proteins lacking available UniProt ID were  
290 also excluded. Datasets that are computationally processed or their wildtype-like and nonsense-  
291 like scores (see Normalization) cannot be identified were also filtered out (Supplementary  
292 Table 1). All missense variants with only a single amino acid substitution were curated from  
293 the DMS studies for our analysis. A total of 130 DMS experiments from 53 studies [5,6,9–  
294 14,27,33–35,38,57–94] were collected for our analysis.

295

### 296 **9.2 Collection of AS data and other features**

297 The following process was used to search for candidate AS studies. Papers were identified by  
298 searching on PubMed and Google Scholar for the “alanine scan” or “alanine scanning” together  
299 with the name of candidate proteins. While searching in Google Scholar, we included the  
300 protein’s UniProt ID rather than molecule name as the search term to reduce false positives.  
301 Appropriate AS data were collected from the search results. Western blot results were  
302 transformed to values by ImageJ if it was the only experimental data available in the study. A  
303 total 146 AS experiments were collected from 45 distinct studies [22–24,26,27,39–  
304 42,44,45,84,95–127].

305 Protein features of Shannon entropy and the logarithm of variant amino acid frequency were  
306 downloaded from the DeMaSk online toolkit [17]. The substitution score matrix feature was  
307 calculated from the mean of training DMS scores for each of the 380 possible amino acid  
308 substitutions before each iteration of cross-validation.

309

### 310 **9.3 Normalization**

311 DMS and AS datasets were normalized to a common scale using the following approach  
312 adapted from previous studies [15,43]. Let  $D$  denotes a protein study measuring scores  $s_i^D$  for  
313 a single variant  $i$ ,  $s_{wt}^D$  denotes the scores for wildtype and  $s_{non}^D$  represents the score for  
314 nonsense-like variants. The normalized scores  $s_i'^D$  are given by:

$$315 \quad s_i'^D := \frac{s_i^D - s_{wt}^D}{s_{wt}^D - s_{non}^D} + 1$$

316 Wild-type scores were directly identified from the paper or the median score of synonymous  
317 variants. For DMS data, since not all DMS studies report score of nonsense variants, we defined  
318 the nonsense-like scores as the median DMS scores for the 1% missense variants with the  
319 strongest loss of function for each dataset. For AS data, nonsense-like scores were either  
320 defined according to the paper or using the extreme values (Supplementary Table 1).

321

### 322 **9.4 AS data filtering and matching**

323 AS data subsets were filtered/matched according to either assay compatibility or score  
324 correlation. For assay compatibility filtering, DMS and AS assay pairs were first classified into  
325 three levels of compatibility (Fig S2). For each DMS dataset, we first tried to use only AS data  
326 with high assay compatibility for further modelling, removing AS data of medium and low  
327 assay compatibility. We then also tried to model with AS data of both high and medium assay  
328 compatibility.

329 For score correlation matching, Spearman's correlation ( $\rho$ ) is calculated between alanine  
330 substitution scores in each pair of AS and DMS data. To avoid influence from the size of AS  
331 datasets, we regularised the  $\rho$  value by empirical copula [128]:

$$332 \quad \rho_r := \rho \times \frac{n-1}{n+1}$$

333 where  $\rho_r$  is the regularised correlation coefficient, and  $n$  is the number of alanine substitutions  
334 used for correlation calculation. For each DMS dataset, AS result with the highest  $\rho_r$  was  
335 picked for modelling.

336

### 337 **9.5 AS data pre-processing**

338 AS data were pre-processed prior to modelling. For variants without available  
339 (filtered/matched) AS data, their AS scores were imputed with the mean value of all available  
340 AS scores. Then the AS data were encoded by the wild-type and variant amino acid type with  
341 one-hot-encoding. For each variant, the AS feature is expanded with two one-hot vectors. Each  
342 of the vectors has 19 zeros and one non-zero value which was the AS score, with the location  
343 of the non-zero value indicating the wild-type or variant amino acid type.

344

### 345 **9.6 Training and evaluation of DMS score predictor**

346 To build the predictors, we performed linear regression using the function  
347 `sklearn.linear_model.LinearRegression` from scikit-learn [129]. Training and  
348 validation data were separated with leave-one-protein-out cross-validation. In this process, data  
349 from one protein were withheld for subsequent validation, and the rest were used for training.  
350 This process was iterated over all proteins in the data. Variants were inversely weighted during  
351 the training process by the number of measurements available, thus compensating for some  
352 regions having greater coverage with DMS and AS assays. Predictors were trained on protein  
353 features, DMS data and (optionally) AS data using four different filtering or matching  
354 strategies: i) all DMS/AS data, ii) compatibility-filtered DMS/AS data, iii) correlation-matched  
355 DMS/AS data, and iv) a control, constructed using DMS data only.

356 In the evaluation process, let  $V$  be protein variants assayed by both DMS study  $D$  and AS study  
357  $A$ . Variant scores are predicted by the previously mentioned predictors either using AS data

358 ( $\hat{s}_V^A$ ) or not ( $\hat{s}_V$ ). Spearman's correlation ( $\rho$ ) was calculated between the DMS scores  $s_V^D$  and  
359 each set of predicted scores. The difference of  $\rho$  was used to evaluate the performance change  
360 ( $\Delta\rho_V$ ).

$$361 \quad \rho_V^A = \text{Spearman's correlation}(\hat{s}_V^A, s_V^D)$$

$$362 \quad \rho_V = \text{Spearman's correlation}(\hat{s}_V, s_V^D)$$

$$363 \quad \Delta\rho_V = \rho_V^A - \rho_V$$

364 To evaluate, we iterated over variants from each pair of DMS/AS studies. Results were dropped  
365 for variants  $V$  with only one protein residue available during analysis and visualization.

366

## 367 **10 References**

368 1. Fowler DM, Fields S. Deep mutational scanning: a new style of protein science. *Nature*  
369 *Methods*. 2014; doi: 10.1038/nmeth.3027.

370 2. Findlay GM. Linking genome variants to disease: scalable approaches to test the functional  
371 impact of human mutations. *Human Molecular Genetics*. 2021; doi: 10.1093/hmg/ddab219.

372 3. Geck RC, Boyle G, Amorosi CJ, Fowler DM, Dunham MJ. Measuring Pharmacogene  
373 Variant Function at Scale Using Multiplexed Assays. *Annual Review of Pharmacology and*  
374 *Toxicology*. 2022; doi: 10.1146/annurev-pharmtox-032221-085807.

375 4. Weile J, Roth FP. Multiplexed assays of variant effects contribute to a growing genotype–  
376 phenotype atlas. *Hum Genet*. 2018; doi: 10.1007/s00439-018-1916-x.

377 5. Diss G, Lehner B. The genetic landscape of a physical interaction. *eLife*. 2018; doi:  
378 10.7554/eLife.32472.

- 379 6. Fowler DM, Araya CL, Fleishman SJ, Kellogg EH, Stephany JJ, Baker D, et al.. High-  
380 resolution mapping of protein sequence-function relationships. *Nature Methods*. 2010; doi:  
381 10.1038/nmeth.1492.
- 382 7. Amorosi CJ, Chiasson MA, McDonald MG, Wong LH, Sitko KA, Boyle G, et al.. Massively  
383 parallel characterization of CYP2C9 variant enzyme activity and abundance. *The American*  
384 *Journal of Human Genetics*. 2021; doi: 10.1016/j.ajhg.2021.07.001.
- 385 8. Faure AJ, Domingo J, Schmiedel JM, Hidalgo-Carcedo C, Diss G, Lehner B. Mapping the  
386 energetic and allosteric landscapes of protein binding domains. *Nature*. 2022; doi:  
387 10.1038/s41586-022-04586-4.
- 388 9. Matreyek KA, Starita LM, Stephany JJ, Martin B, Chiasson MA, Gray VE, et al.. Multiplex  
389 assessment of protein variant abundance by massively parallel sequencing. *Nature Genetics*.  
390 2018; doi: 10.1038/s41588-018-0122-z.
- 391 10. Mighell TL, Evans-Dutson S, O’Roak BJ. A Saturation Mutagenesis Approach to  
392 Understanding PTEN Lipid Phosphatase Activity and Genotype-Phenotype Relationships. *The*  
393 *American Journal of Human Genetics*. 2018; doi: 10.1016/j.ajhg.2018.03.018.
- 394 11. Stiffler MA, Hekstra DR, Ranganathan R. Evolvability as a Function of Purifying Selection  
395 in TEM-1  $\beta$ -Lactamase. *Cell*. 2015; doi: 10.1016/j.cell.2015.01.035.
- 396 12. Ahler E, Register AC, Chakraborty S, Fang L, Dieter EM, Sitko KA, et al.. A Combined  
397 Approach Reveals a Regulatory Mechanism Coupling Src’s Kinase Activity, Localization, and  
398 Phosphotransferase-Independent Functions. *Molecular Cell*. 2019; doi:  
399 10.1016/j.molcel.2019.02.003.

- 400 13. Giacomelli AO, Yang X, Lintner RE, McFarland JM, Duby M, Kim J, et al.. Mutational  
401 processes shape the landscape of TP53 mutations in human cancer. *Nature Genetics*. Nature  
402 Publishing Group; 2018; doi: 10.1038/s41588-018-0204-y.
- 403 14. Roscoe BP, Thayer KM, Zeldovich KB, Fushman D, Bolon DNA. Analyses of the Effects  
404 of All Ubiquitin Point Mutants on Yeast Growth Rate. *Journal of Molecular Biology*. 2013;  
405 doi: 10.1016/j.jmb.2013.01.032.
- 406 15. Gray VE, Hause RJ, Luebeck J, Shendure J, Fowler DM. Quantitative Missense Variant  
407 Effect Prediction Using Large-Scale Mutagenesis Data. *Cell Systems*. 2018; doi:  
408 10.1016/j.cels.2017.11.003.
- 409 16. Alley EC, Khimulya G, Biswas S, AlQuraishi M, Church GM. Unified rational protein  
410 engineering with sequence-based deep representation learning. *Nat Methods*. 2019; doi:  
411 10.1038/s41592-019-0598-1.
- 412 17. Munro D, Singh M. DeMaSk: a deep mutational scanning substitution matrix and its use  
413 for variant impact prediction. Xu J, editor. *Bioinformatics*. 2020; doi:  
414 10.1093/bioinformatics/btaa1030.
- 415 18. Biswas S, Khimulya G, Alley EC, Esvelt KM, Church GM. Low- N protein engineering  
416 with data-efficient deep learning. *Nature Methods*. Nature Publishing Group; 2021; doi:  
417 10.1038/s41592-021-01100-y.
- 418 19. Høie MH, Cagiada M, Beck Frederiksen AH, Stein A, Lindorff-Larsen K. Predicting and  
419 interpreting large-scale mutagenesis data using analyses of protein stability and conservation.  
420 *Cell Reports*. 2022; doi: 10.1016/j.celrep.2021.110207.

421 20. Wu Y, Li R, Sun S, Weile J, Roth FP. Improved pathogenicity prediction for rare human  
422 missense variants. *The American Journal of Human Genetics*. 2021; doi:  
423 10.1016/j.ajhg.2021.08.012.

424 21. Hsu C, Nisonoff H, Fannjiang C, Listgarten J. Learning protein fitness models from  
425 evolutionary and assay-labeled data. *Nat Biotechnol*. 2022; doi: 10.1038/s41587-021-01146-5.

426 22. Block C, Janknecht R, Herrmann C, Nassar N, Wittinghofer A. Quantitative structure-  
427 activity analysis correlating Ras/Raf interaction in vitro to Raf activation in vivo. *Nature*  
428 *Structural Biology*. Nature Publishing Group; 1996; doi: 10.1038/nsb0396-244.

429 23. Sloan DJ, Hellinga HW. Dissection of the protein G B1 domain binding site for human IgG  
430 Fc fragment. *Protein Science*. 1999; doi: 10.1110/ps.8.8.1643.

431 24. Fleming KG, Engelman DM. Specificity in transmembrane helix–helix interactions can  
432 define a hierarchy of stability for sequence variants. *PNAS*. National Academy of Sciences;  
433 2001; doi: 10.1073/pnas.251367498.

434 25. Shibata Y, White JF, Serrano-Vega MJ, Magnani F, Aloia AL, Grisshammer R, et al..  
435 Thermostabilization of the Neurotensin Receptor NTS1. *Journal of Molecular Biology*. 2009;  
436 doi: 10.1016/j.jmb.2009.04.068.

437 26. Brzovic PS, Heikaus CC, Kisselev L, Vernon R, Herbig E, Pacheco D, et al.. The Acidic  
438 Transcription Activator Gcn4 Binds the Mediator Subunit Gal11/Med15 Using a Simple  
439 Protein Interface Forming a Fuzzy Complex. *Molecular Cell*. 2011; doi:  
440 10.1016/j.molcel.2011.11.008.



- 441 27. Gajula KS, Huwe PJ, Mo CY, Crawford DJ, Stivers JT, Radhakrishnan R, et al.. High-  
442 throughput mutagenesis reveals functional determinants for DNA targeting by activation-  
443 induced deaminase. *Nucleic Acids Research*. 2014; doi: 10.1093/nar/gku689.
- 444 28. Kortemme T, Kim DE, Baker D. Computational Alanine Scanning of Protein-Protein  
445 Interfaces. *Science's STKE*. American Association for the Advancement of Science; 2004; doi:  
446 10.1126/stke.2192004pl2.
- 447 29. Morrison KL, Weiss GA. Combinatorial alanine-scanning. *Current Opinion in Chemical*  
448 *Biology*. 2001; doi: 10.1016/S1367-5931(00)00206-4.
- 449 30. Cunningham BC, Wells JA. High-resolution epitope mapping of hGH-receptor interactions  
450 by alanine-scanning mutagenesis. *Science*. American Association for the Advancement of  
451 Science; 1989; doi: 10.1126/science.2471267.
- 452 31. DeLano WL. Unraveling hot spots in binding interfaces: progress and challenges. *Current*  
453 *Opinion in Structural Biology*. 2002; doi: 10.1016/S0959-440X(02)00283-X.
- 454 32. Eustache S, Leprince J, Tufféry P. Progress with peptide scanning to study structure-  
455 activity relationships: the implications for drug discovery. *Expert Opinion on Drug Discovery*.  
456 2016; doi: 10.1080/17460441.2016.1201058.
- 457 33. Olson CA, Wu NC, Sun R. A Comprehensive Biophysical Description of Pairwise Epistasis  
458 throughout an Entire Protein Domain. *Current Biology*. 2014; doi: 10.1016/j.cub.2014.09.072.
- 459 34. Staller MV, Holehouse AS, Swain-Lenz D, Das RK, Pappu RV, Cohen BA. A High-  
460 Throughput Mutational Scan of an Intrinsically Disordered Acidic Transcriptional Activation  
461 Domain. *Cell Systems*. 2018; doi: 10.1016/j.cels.2018.01.015.

462 35. Gray VE, Sitko K, Kameni FZN, Williamson M, Stephany JJ, Hasle N, et al.. Elucidating  
463 the Molecular Determinants of A $\beta$  Aggregation with Deep Mutational Scanning. *G3*  
464 (*Bethesda*). 2019; doi: 10.1534/g3.119.400535.

465 36. Esposito D, Weile J, Shendure J, Starita LM, Papenfuss AT, Roth FP, et al.. MaveDB: an  
466 open-source platform to distribute and interpret data from multiplexed assays of variant effect.  
467 *Genome Biol.* 2019; doi: 10.1186/s13059-019-1845-6.

468 37. Rubin AF, Min JK, Rollins NJ, Da EY, Esposito D, Harrington M, et al.. MaveDB v2: a  
469 curated community database with over three million variant effects from multiplexed  
470 functional assays. bioRxiv;

471 38. Heredia JD, Park J, Brubaker RJ, Szymanski SK, Gill KS, Procko E. Mapping Interaction  
472 Sites on Human Chemokine Receptors by Deep Mutational Scanning. *The Journal of*  
473 *Immunology*. American Association of Immunologists; 2018; doi: 10.4049/jimmunol.1800343.

474 39. Tian S, Choi W-T, Liu D, Pesavento J, Wang Y, An J, et al.. Distinct Functional Sites for  
475 Human Immunodeficiency Virus Type 1 and Stromal Cell-Derived Factor 1 $\alpha$  on CXCR4  
476 Transmembrane Helical Domains. *JVI.* 2005; doi: 10.1128/JVI.79.20.12667-12673.2005.

477 40. Chabot DJ, Zhang P-F, Quinnan GV, Broder CC. Mutagenesis of CXCR4 Identifies  
478 Important Domains for Human Immunodeficiency Virus Type 1 X4 Isolate Envelope-  
479 Mediated Membrane Fusion and Virus Entry and Reveals Cryptic Coreceptor Activity for R5  
480 Isolates. *J Virol.* 1999; doi: 10.1128/JVI.73.8.6598-6609.1999.

481 41. Han DP, Penn-Nicholson A, Cho MW. Identification of critical determinants on ACE2 for  
482 SARS-CoV entry and development of a potent entry inhibitor. *Virology.* 2006; doi:  
483 10.1016/j.virol.2006.01.029.

484 42. Fujita–Yoshigaki J, Shirouzu M, Ito Y, Hattori S, Furuyama S, Nishimura S, et al.. A  
485 Constitutive Effector Region on the C-terminal Side of Switch I of the Ras Protein. *J Biol Chem.*  
486 American Society for Biochemistry and Molecular Biology; 1995; doi: 10.1074/jbc.270.9.4661.

487 43. Gray VE, Hause RJ, Fowler DM. Analysis of Large-Scale Mutagenesis Data To Assess the  
488 Impact of Single Amino Acid Substitutions. *Genetics.* 2017; doi: 10.1534/genetics.117.300064.

489 44. Hidalgo P, Ansari AZ, Schmidt P, Hare B, Simkovich N, Farrell S, et al.. Recruitment of  
490 the transcriptional machinery through GAL11P: structure and interactions of the GAL4  
491 dimerization domain. *Genes Dev.* 2001; doi: 10.1101/gad.873901.

492 45. Rodríguez-Escudero I, Oliver MD, Andrés-Pons A, Molina M, Cid VJ, Pulido R. A  
493 comprehensive functional analysis of PTEN mutations: implications in tumor- and autism-  
494 related syndromes. *Human Molecular Genetics.* 2011; doi: 10.1093/hmg/ddr337.

495 46. Schröter C, Günther R, Rhiel L, Becker S, Toleikis L, Doerner A, et al.. A generic approach  
496 to engineer antibody pH-switches using combinatorial histidine scanning libraries and yeast  
497 display. *mAbs.* 2015; doi: 10.4161/19420862.2014.985993.

498 47. Starace DM, Bezanilla F. Histidine Scanning Mutagenesis of Basic Residues of the S4  
499 Segment of the Shaker K<sup>+</sup> Channel. *J Gen Physiol.* 117:469–902001;

500 48. Stekhoven DJ, Buhlmann P. MissForest--non-parametric missing value imputation for  
501 mixed-type data. *Bioinformatics.* 2012; doi: 10.1093/bioinformatics/btr597.

502 49. Wu Y, Weile J, Cote AG, Sun S, Knapp J, Verby M, et al.. A web application and service  
503 for imputing and visualizing missense variant effect maps. Schwartz R, editor. *Bioinformatics.*  
504 2019; doi: 10.1093/bioinformatics/btz012.

505 50. Cagiada M, Johansson KE, Valanciute A, Nielsen SV, Hartmann-Petersen R, Yang JJ, et  
506 al.. Understanding the Origins of Loss of Protein Function by Analyzing the Effects of  
507 Thousands of Variants on Activity and Abundance. Ozkan B, editor. *Molecular Biology and*  
508 *Evolution*. 2021; doi: 10.1093/molbev/msab095.

509 51. Cagiada M, Bottaro S, Lindemose S, Schenstrøm SM, Stein A, Hartmann-Petersen R, et  
510 al.. Discovering functionally important sites in proteins. bioRxiv;

511 52. Jepsen MM, Fowler DM, Hartmann-Petersen R, Stein A, Lindorff-Larsen K. Chapter 5 -  
512 Classifying disease-associated variants using measures of protein activity and stability. In: Pey  
513 AL, editor. *Protein Homeostasis Diseases*. Academic Press;

514 53. Matreyek KA, Stephany JJ, Ahler E, Fowler DM. Integrating thousands of PTEN variant  
515 activity and abundance measurements reveals variant subgroups and new dominant negatives  
516 in cancers. *Genome Med*. 2021; doi: 10.1186/s13073-021-00984-x.

517 54. Mighell TL, Thacker S, Fombonne E, Eng C, O’Roak BJ. An Integrated Deep-Mutational-  
518 Scanning Approach Provides Clinical Insights on PTEN Genotype-Phenotype Relationships.  
519 *The American Journal of Human Genetics*. 2020; doi: 10.1016/j.ajhg.2020.04.014.

520 55. Nielsen SV, Hartmann-Petersen R, Stein A, Lindorff-Larsen K. Multiplexed assays reveal  
521 effects of missense variants in MSH2 and cancer predisposition. *PLOS Genetics*. Public  
522 Library of Science; 2021; doi: 10.1371/journal.pgen.1009496.

523 56. The UniProt Consortium, Bateman A, Martin M-J, Orchard S, Magrane M, Agivetova R,  
524 et al.. UniProt: the universal protein knowledgebase in 2021. *Nucleic Acids Research*. 2021;  
525 doi: 10.1093/nar/gkaa1100.

526 57. Andrews B, Fields S. Distinct patterns of mutational sensitivity for  $\lambda$  resistance and  
527 maltodextrin transport in *Escherichia coli* LamB. *Microb Genom.* 2020; doi:  
528 10.1099/mgen.0.000364.

529 58. Bandaru P, Shah NH, Bhattacharyya M, Barton JP, Kondo Y, Cofsky JC, et al..  
530 Deconstruction of the Ras switching cycle through saturation mutagenesis. *eLife.* 2017; doi:  
531 10.7554/eLife.27810.

532 59. Bolognesi B, Faure AJ, Seuma M, Schmiedel JM, Tartaglia GG, Lehner B. The mutational  
533 landscape of a prion-like domain. *Nat Commun.* 2019; doi: 10.1038/s41467-019-12101-z.

534 60. Bridgford JL, Lee SM, Lee CMM, Guglielmelli P, Rumi E, Pietra D, et al.. Novel drivers  
535 and modifiers of MPL-dependent oncogenic transformation identified by deep mutational  
536 scanning. *Blood.* American Society of Hematology; 2020; doi: 10.1182/blood.2019002561.

537 61. Chan KK, Dorosky D, Sharma P, Abbasi SA, Dye JM, Kranz DM, et al.. Engineering  
538 human ACE2 to optimize binding to the spike protein of SARS coronavirus 2. *Science.*  
539 American Association for the Advancement of Science; 2020; doi: 10.1126/science.abc0870.

540 62. Chiasson MA, Rollins NJ, Stephany JJ, Sitko KA, Matreyek KA, Verby M, et al..  
541 Multiplexed measurement of variant abundance and activity reveals VKOR topology, active  
542 site and human variant impact. *Elife.* 2020; doi: 10.7554/eLife.58026.

543 63. Elazar A, Weinstein J, Biran I, Fridman Y, Bibi E, Fleishman SJ. Mutational scanning  
544 reveals the determinants of protein insertion and association energetics in the plasma  
545 membrane. Shan Y, editor. *eLife.* eLife Sciences Publications, Ltd; 2016; doi:  
546 10.7554/eLife.12125.

- 547 64. Findlay GM, Daza RM, Martin B, Zhang MD, Leith AP, Gasperini M, et al.. Accurate  
548 classification of BRCA1 variants with saturation genome editing. *Nature*. 2018; doi:  
549 10.1038/s41586-018-0461-z.
- 550 65. Firnberg E, Labonte JW, Gray JJ, Ostermeier M. A Comprehensive, High-Resolution Map  
551 of a Gene's Fitness Landscape. *Mol Biol Evol*. 2014; doi: 10.1093/molbev/msu081.
- 552 66. Hietpas RT, Jensen JD, Bolon DNA. Experimental illumination of a fitness landscape.  
553 *Proceedings of the National Academy of Sciences*. 2011; doi: 10.1073/pnas.1016024108.
- 554 67. Hietpas RT, Bank C, Jensen JD, Bolon DNA. Shifting fitness landscapes in response to  
555 altered environments. *Evolution*. 2013; doi: 10.1111/evo.12207.
- 556 68. Jiang L, Mishra P, Hietpas RT, Zeldovich KB, Bolon DNA. Latent Effects of Hsp90  
557 Mutants Revealed at Reduced Expression Levels. *PLOS Genetics*. Public Library of Science;  
558 2013; doi: 10.1371/journal.pgen.1003600.
- 559 69. Jiang RJ. Exhaustive Mapping of Missense Variation in Coronary Heart Disease-related  
560 Genes [Thesis]. University of Toronto;
- 561 70. Keskin A, Akdoğan E, Dunn CD. Evidence for Amino Acid Snorkeling from a High-  
562 Resolution, *In Vivo* Analysis of Fis1 Tail-Anchor Insertion at the Mitochondrial Outer  
563 Membrane. *Genetics*. 2017; doi: 10.1534/genetics.116.196428.
- 564 71. Kitzman JO, Starita LM, Lo RS, Fields S, Shendure J. Massively parallel single-amino-  
565 acid mutagenesis. *Nat Methods*. 2015; doi: 10.1038/nmeth.3223.
- 566 72. Kotler E, Shani O, Goldfeld G, Lotan-Pompan M, Tarcic O, Gershoni A, et al.. A  
567 Systematic p53 Mutation Library Links Differential Functional Impact to Cancer Mutation

568 Pattern and Evolutionary Conservation. *Molecular Cell*. Elsevier; 2018; doi:  
569 10.1016/j.molcel.2018.06.012.

570 73. Kowalsky CA, Whitehead TA. Determination of binding affinity upon mutation for type I  
571 dockerin–cohesin complexes from *Clostridium thermocellum* and *Clostridium cellulolyticum*  
572 using deep sequencing. *Proteins: Structure, Function, and Bioinformatics*. 2016; doi:  
573 10.1002/prot.25175.

574 74. McLaughlin Jr RN, Poelwijk FJ, Raman A, Gosal WS, Ranganathan R. The spatial  
575 architecture of protein function and adaptation. *Nature*. 2012; doi: 10.1038/nature11500.

576 75. Melamed D, Young DL, Gamble CE, Miller CR, Fields S. Deep mutational scanning of an  
577 RRM domain of the *Saccharomyces cerevisiae* poly(A)-binding protein. *RNA*. 2013; doi:  
578 10.1261/rna.040709.113.

579 76. Mishra P, Flynn JM, Starr TN, Bolon DNA. Systematic Mutant Analyses Elucidate General  
580 and Client-Specific Aspects of Hsp90 Function. *Cell Reports*. 2016; doi:  
581 10.1016/j.celrep.2016.03.046.

582 77. Nedrud D, Coyote-Maestas W, Schmidt D. A large-scale survey of pairwise epistasis  
583 reveals a mechanism for evolutionary expansion and specialization of PDZ domains. *Proteins:  
584 Structure, Function, and Bioinformatics*. 2021; doi: 10.1002/prot.26067.

585 78. Newberry RW, Arhar T, Costello J, Hartoularos GC, Maxwell AM, Naing ZZC, et al..  
586 Robust Sequence Determinants of  $\alpha$ -Synuclein Toxicity in Yeast Implicate Membrane Binding.  
587 *ACS Chem Biol*. 2020; doi: 10.1021/acscchembio.0c00339.

588 79. Newberry RW, Leong JT, Chow ED, Kampmann M, DeGrado WF. Deep mutational  
589 scanning reveals the structural basis for  $\alpha$ -synuclein activity. *Nat Chem Biol.* 2020; doi:  
590 10.1038/s41589-020-0480-6.

591 80. Roscoe BP, Bolon DNA. Systematic Exploration of Ubiquitin Sequence, E1 Activation  
592 Efficiency, and Experimental Fitness in Yeast. *Journal of Molecular Biology.* 2014; doi:  
593 10.1016/j.jmb.2014.05.019.

594 81. Sarkisyan KS, Bolotin DA, Meer MV, Usmanova DR, Mishin AS, Sharonov GV, et al..  
595 Local fitness landscape of the green fluorescent protein. *Nature.* Nature Publishing Group;  
596 2016; doi: 10.1038/nature17995.

597 82. Silverstein RA, Sun S, Verby M, Weile J, Wu Y, Roth FP. A systematic genotype-  
598 phenotype map for missense variants in the human intellectual disability-associated gene GDI1.  
599 bioRxiv;

600 83. Starita LM, Pruneda JN, Lo RS, Fowler DM, Kim HJ, Hiatt JB, et al.. Activity-enhancing  
601 mutations in an E3 ubiquitin ligase identified by high-throughput mutagenesis. *PNAS.* 2013;  
602 doi: 10.1073/pnas.1303309110.

603 84. Starita LM, Young DL, Islam M, Kitzman JO, Gullingsrud J, Hause RJ, et al.. Massively  
604 Parallel Functional Analysis of BRCA1 RING Domain Variants. *Genetics.* 2015; doi:  
605 10.1534/genetics.115.175802.

606 85. Starita LM, Islam MM, Banerjee T, Adamovich AI, Gullingsrud J, Fields S, et al.. A  
607 Multiplex Homology-Directed DNA Repair Assay Reveals the Impact of More Than 1,000  
608 BRCA1 Missense Substitution Variants on Protein Function. *The American Journal of Human*  
609 *Genetics.* 2018; doi: 10.1016/j.ajhg.2018.07.016.



610 86. Suiter CC, Moriyama T, Matreyek KA, Yang W, Scaletti ER, Nishii R, et al.. Massively  
611 parallel variant characterization identifies *NUDT15* alleles associated with thiopurine toxicity.  
612 *Proc Natl Acad Sci USA*. 2020; doi: 10.1073/pnas.1915680117.

613 87. Sun S, Weile J, Verby M, Wu Y, Wang Y, Cote AG, et al.. A proactive genotype-to-patient-  
614 phenotype map for cystathionine beta-synthase. *Genome Med*. 2020; doi: 10.1186/s13073-020-  
615 0711-1.

616 88. Thompson S, Zhang Y, Ingle C, Reynolds KA, Kortemme T. Altered expression of a quality  
617 control protease in *E. coli* reshapes the in vivo mutational landscape of a model enzyme. *eLife*.  
618 2020; doi: 10.7554/eLife.53476.

619 89. Trenker R, Wu X, Nguyen JV, Wilcox S, Rubin AF, Call ME, et al.. Human and viral  
620 membrane-associated E3 ubiquitin ligases MARCH1 and MIR2 recognize different features  
621 of CD86 to downregulate surface expression. *Journal of Biological Chemistry*. Elsevier; 2021;  
622 doi: 10.1016/j.jbc.2021.100900.

623 90. Weile J, Sun S, Cote AG, Knapp J, Verby M, Mellor JC, et al.. A framework for  
624 exhaustively mapping functional missense variants. *Mol Syst Biol*. 2017; doi:  
625 10.15252/msb.20177908.

626 91. Weile J, Kishore N, Sun S, Maaieh R, Verby M, Li R, et al.. Shifting landscapes of human  
627 MTHFR missense-variant effects. *The American Journal of Human Genetics*. Elsevier; 2021;  
628 doi: 10.1016/j.ajhg.2021.05.009.

629 92. Wrenbeck EE, Bedewitz MA, Klesmith JR, Noshin S, Barry CS, Whitehead TA. An  
630 Automated Data-Driven Pipeline for Improving Heterologous Enzyme Expression. *ACS Synth*  
631 *Biol*. American Chemical Society; 2019; doi: 10.1021/acssynbio.8b00486.

632 93. Zhang L, Sarangi V, Moon I, Yu J, Liu D, Devarajan S, et al.. CYP2C9 and CYP2C19:  
633 Deep Mutational Scanning and Functional Characterization of Genomic Missense Variants.  
634 *Clinical and Translational Science*. 2020; doi: <https://doi.org/10.1111/cts.12758>.

635 94. Zinkus-Boltz J, DeValk C, Dickinson BC. A Phage-Assisted Continuous Selection  
636 Approach for Deep Mutational Scanning of Protein–Protein Interactions. *ACS Chem Biol*.  
637 American Chemical Society; 2019; doi: 10.1021/acscchembio.9b00669.

638 95. Bernier-Villamor V, Sampson DA, Matunis MJ, Lima CD. Structural Basis for E2-  
639 Mediated SUMO Conjugation Revealed by a Complex between Ubiquitin-Conjugating  
640 Enzyme Ubc9 and RanGAP. *Cell*. 108:122002;

641 96. Blanpain C, Doranz BJ, Vakili J, Rucker J, Govaerts C, Baik SSW, et al.. Multiple Charged  
642 and Aromatic Residues in CCR5 Amino-terminal Domain Are Involved in High Affinity  
643 Binding of Both Chemokines and HIV-1 Env Protein. *J Biol Chem*. 1999; doi:  
644 10.1074/jbc.274.49.34719.

645 97. Brzovic PS, Keefe JR, Nishikawa H, Miyamoto K, Fox D, Fukuda M, et al.. Binding and  
646 recognition in the assembly of an active BRCA1/BARD1 ubiquitin-ligase complex.  
647 *Proceedings of the National Academy of Sciences*. 2003; doi: 10.1073/pnas.0836054100.

648 98. Chen S, Wu J, Zhong S, Li Y, Zhang P, Ma J, et al.. iASPP mediates p53 selectivity through  
649 a modular mechanism fine-tuning DNA recognition. *Proc Natl Acad Sci USA*. 2019; doi:  
650 10.1073/pnas.1909393116.

651 99. Chupreta S, Holmstrom S, Subramanian L, Iñiguez-Lluhí JA. A Small Conserved Surface  
652 in SUMO Is the Critical Structural Determinant of Its Transcriptional Inhibitory Properties.  
653 *MCB*. 2005; doi: 10.1128/MCB.25.10.4272-4282.2005.

654 100. Cobb JA, Roberts DM. Structural Requirements for N-Trimethylation of Lysine 115 of  
655 Calmodulin. *Journal of Biological Chemistry*. 2000; doi: 10.1074/jbc.M002332200.

656 101. Coyne RS, McDonald HB, Edgemon K, Brody LC. Functional Characterization of  
657 BRCA1 Sequence Variants using a Yeast Small Colony Phenotype Assay. *Cancer Biology &*  
658 *Therapy*. 2004; doi: 10.4161/cbt.3.5.809.

659 102. Denker K, Orlik F, Schiffler B, Benz R. Site-directed Mutagenesis of the Greasy Slide  
660 Aromatic Residues Within the LamB (Maltoporin) Channel of Escherichia coli: Effect on Ion  
661 and Maltopentaose Transport. *Journal of Molecular Biology*. 2005; doi:  
662 10.1016/j.jmb.2005.07.025.

663 103. Dragic T, Trkola A, Lin SW, Nagashima KA, Kajumo F, Zhao L, et al.. Amino-Terminal  
664 Substitutions in the CCR5 Coreceptor Impair gp120 Binding and Human Immunodeficiency  
665 Virus Type 1 Entry. *J Virol*. 1998; doi: 10.1128/JVI.72.1.279-285.1998.

666 104. Dragic T, Trkola A, Thompson DAD, Cormier EG, Kajumo FA, Maxwell E, et al.. A  
667 binding pocket for a small molecule inhibitor of HIV-1 entry within the transmembrane helices  
668 of CCR5. *Proceedings of the National Academy of Sciences*. 2000; doi:  
669 10.1073/pnas.090576697.

670 105. Ecsédi P, Gógl G, Hóf H, Kiss B, Harmat V, Nyitray L. Structure Determination of the  
671 Transactivation Domain of p53 in Complex with S100A4 Using Annexin A2 as a  
672 Crystallization Chaperone. *Structure*. 2020; doi: 10.1016/j.str.2020.05.001.

673 106. Kopecká J, Krijt J, Raková K, Kožich V. Restoring assembly and activity of cystathionine  
674  $\beta$ -synthase mutants by ligands and chemical chaperones. *Journal of Inherited Metabolic*  
675 *Disease*. 2011; doi: 10.1007/s10545-010-9087-5.

676 107. Kožich V, Sokolová J, Klatovská V, Krijt J, Janošík M, Jelínek K, et al.. Cystathionine  $\beta$ -  
677 synthase mutations: effect of mutation topology on folding and activity. *Hum Mutat.* 2010; doi:  
678 10.1002/humu.21273.

679 108. Kruger W d., Wang L, Jhee K h., Singh R h., Elsas II L j.. Cystathionine  $\beta$ -synthase  
680 deficiency in Georgia (USA): Correlation of clinical and biochemical phenotype with genotype.  
681 *Human Mutation.* 2003; doi: 10.1002/humu.10290.

682 109. Lee SY, Pullen L, Virgil DJ, Castañeda CA, Abeykoon D, Bolon DNA, et al.. Alanine  
683 Scan of Core Positions in Ubiquitin Reveals Links between Dynamics, Stability, and Function.  
684 *Journal of Molecular Biology.* 2014; doi: 10.1016/j.jmb.2013.10.042.

685 110. Li W, Zhang C, Sui J, Kuhn JH, Moore MJ, Luo S, et al.. Receptor and viral determinants  
686 of SARS-coronavirus adaptation to human ACE2. *EMBO J.* 2005; doi:  
687 10.1038/sj.emboj.7600640.

688 111. Lin G, Baribaud F, Romano J, Doms RW, Hoxie JA. Identification of gp120 Binding Sites  
689 on CXCR4 by Using CD4-Independent Human Immunodeficiency Virus Type 2 Env Proteins.  
690 *JVI.* 2003; doi: 10.1128/JVI.77.2.931-942.2003.

691 112. Mascle XH, Lussier-Price M, Cappadocia L, Estephan P, Raiola L, Omichinski JG, et al..  
692 Identification of a Non-covalent Ternary Complex Formed by PIAS1, SUMO1, and UBC9  
693 Proteins Involved in Transcriptional Regulation. *Journal of Biological Chemistry.* 2013; doi:  
694 10.1074/jbc.M113.486845.

695 113. Matthews EE, Thévenin D, Rogers JM, Gotow L, Lira PD, Reiter LA, et al..  
696 Thrombopoietin receptor activation: transmembrane helix dimerization, rotation, and allosteric  
697 modulation. *The FASEB Journal.* 2011; doi: <https://doi.org/10.1096/fj.10-178673>.

698 114. Mayfield JA, Davies MW, Dimster-Denk D, Pleskac N, McCarthy S, Boydston EA, et al..  
699 Surrogate Genetics and Metabolic Profiling for Characterization of Human Disease Alleles.  
700 *Genetics*. 2012; doi: 10.1534/genetics.111.137471.

701 115. Navenot J-M, Wang Z, Trent JO, Murray JL, Hu Q, DeLeeuw L, et al.. Molecular anatomy  
702 of CCR5 engagement by physiologic and viral chemokines and HIV-1 envelope glycoproteins:  
703 differences in primary structural requirements for RANTES, MIP-1 $\alpha$ , and vMIP-II  
704 binding11Edited by P. E. Wright. *Journal of Molecular Biology*. 2001; doi:  
705 10.1006/jmbi.2001.5086.

706 116. Peng L, Damschroder MM, Cook KE, Wu H, Dall'Acqua WF. Molecular basis for the  
707 antagonistic activity of an anti-CXCR4 antibody. *mAbs*. 2016; doi:  
708 10.1080/19420862.2015.1113359.

709 117. Peterson BR, Sun LJ, Verdine GL. A critical arginine residue mediates cooperativity in  
710 the contact interface between transcription factors NFAT and AP-1. *Proceedings of the*  
711 *National Academy of Sciences*. 1996; doi: 10.1073/pnas.93.24.13671.

712 118. Rabut GEE, Konner JA, Kajumo F, Moore JP, Dragic T. Alanine Substitutions of Polar  
713 and Nonpolar Residues in the Amino-Terminal Domain of CCR5 Differently Impair Entry of  
714 Macrophage- and Dualtropic Isolates of Human Immunodeficiency Virus Type 1. *J Virol*. 1998;  
715 doi: 10.1128/JVI.72.4.3464-3468.1998.

716 119. Ransburgh DJR, Chiba N, Ishioka C, Toland AE, Parvin JD. Identification of Breast  
717 Tumor Mutations in *BRCA1* That Abolish Its Function in Homologous DNA Recombination.  
718 *Cancer Res*. 2010; doi: 10.1158/0008-5472.CAN-09-2850.

719 120. Tan Y, Tong P, Wang J, Zhao L, Li J, Yu Y, et al.. The Membrane-Proximal Region of  
720 C–C Chemokine Receptor Type 5 Participates in the Infection of HIV-1. *Front Immunol.* 2017;  
721 doi: 10.3389/fimmu.2017.00478.

722 121. Towler WI, Zhang J, Ransburgh DJR, Toland AE, Ishioka C, Chiba N, et al.. Analysis of  
723 BRCA1 Variants in Double-Strand Break Repair by Homologous Recombination and Single-  
724 Strand Annealing. *Human Mutation.* 2013; doi: 10.1002/humu.22251.

725 122. Trent JO, Wang Z, Murray JL, Shao W, Tamamura H, Fujii N, et al.. Lipid Bilayer  
726 Simulations of CXCR4 with Inverse Agonists and Weak Partial Agonists. *J Biol Chem.* 2003;  
727 doi: 10.1074/jbc.M307850200.

728 123. Van Gelder P, Dumas F, Bartoldus I, Saint N, Prilipov A, Winterhalter M, et al.. Sugar  
729 Transport through Maltoporin of *Escherichia coli* : Role of the Greasy Slide. *J Bacteriol.* 2002;  
730 doi: 10.1128/JB.184.11.2994-2999.2002.

731 124. VanBerkum MF, Means AR. Three amino acid substitutions in domain I of calmodulin  
732 prevent the activation of chicken smooth muscle myosin light chain kinase. *J Biol Chem.*  
733 American Society for Biochemistry and Molecular Biology; 266:21488–951991;

734 125. Wei Q, Wang L, Wang Q, Kruger WD, Dunbrack RL. Testing computational prediction  
735 of missense mutation phenotypes: Functional characterization of 204 mutations of human  
736 cystathionine beta synthase. *Proteins: Structure, Function, and Bioinformatics.* 2010; doi:  
737 10.1002/prot.22722.

738 126. Williams AD, Shivaprasad S, Wetzel R. Alanine Scanning Mutagenesis of A $\beta$ (1-40)  
739 Amyloid Fibril Stability. *Journal of Molecular Biology.* 2006; doi: 10.1016/j.jmb.2006.01.041.

740 127. Zhang J, Rao E, Dioszegi M, Kondru R, DeRosier A, Chan E, et al.. The Second  
741 Extracellular Loop of CCR5 Contains the Dominant Epitopes for Highly Potent Anti-Human  
742 Immunodeficiency Virus Monoclonal Antibodies. *AAC*. 2007; doi: 10.1128/AAC.01302-06.

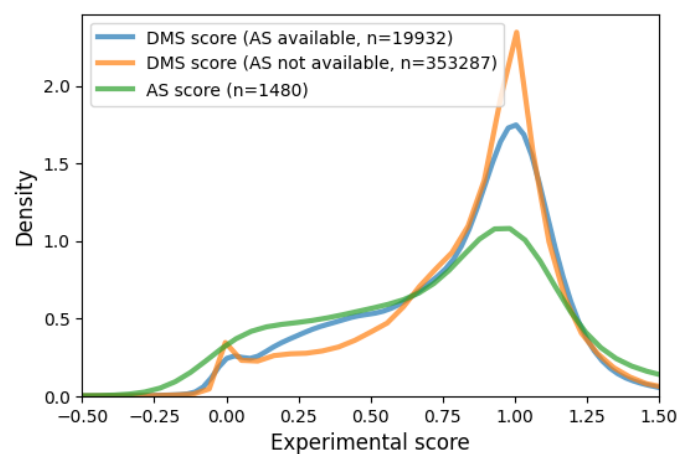
743 128. Nelsen RB. *An introduction to copulas*. 2nd ed. New York: Springer;

744 129. Pedregosa F, Varoquaux G, Gramfort A, Michel V, Thirion B, Grisel O, et al.. Scikit-  
745 learn: Machine Learning in Python. *Journal of machine Learning research*. :2825–30 2011;

746 130. González J, Dai Z, Hennig P, Lawrence ND. Batch Bayesian Optimization via Local  
747 Penalization. arXiv;

748

## 749 **Supplementary material**

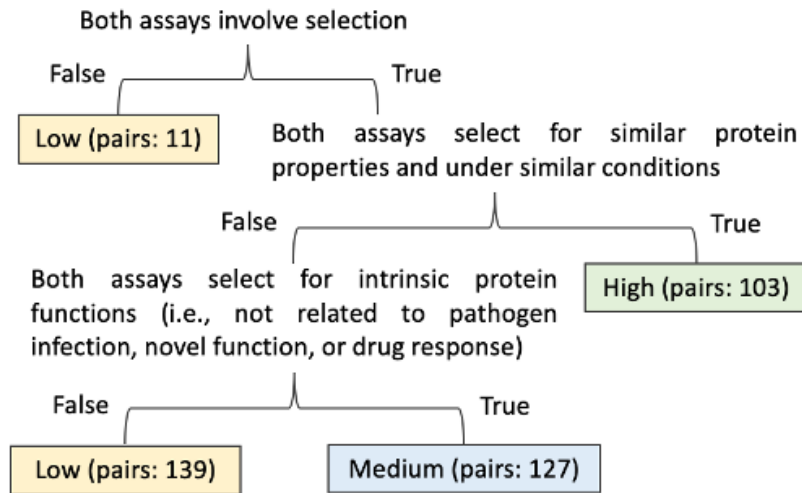


750

751 **Fig S1. DMS and AS score distribution.** The figure shows the kernel estimated density of normalized AS scores  
752 and DMS scores for variants with or without available AS data.

753

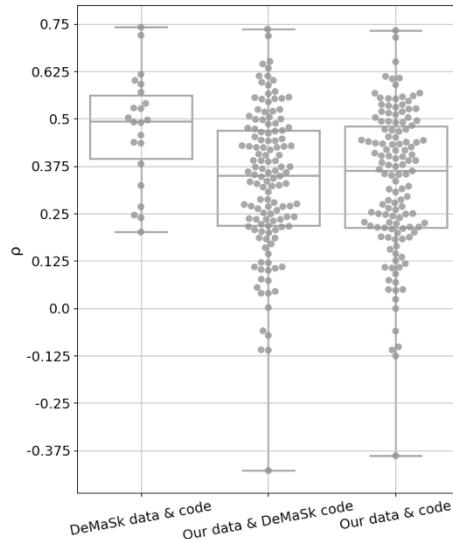
For each **pair** of DMS and AS experiments:



754

755 **Fig S2. Decision tree for classifying the DMS and AS assay compatibility.** The end-nodes show the classified  
756 assay compatibility. The number indicates the count of assay pairs for each compatibility level (low, medium,  
757 high).

758



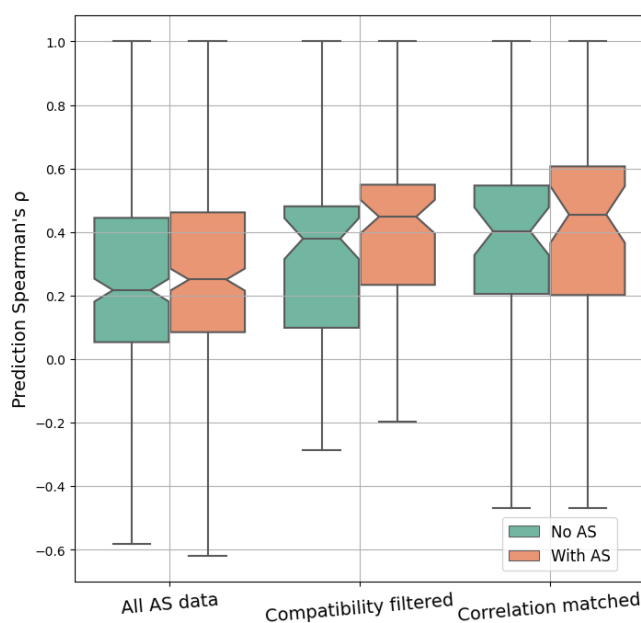
759

760 **Fig S3. Comparison between published and re-implemented predictors.** The plot shows leave-one-protein-  
761 out cross-validation performance on predictors built from the published DeMaSk code or our code. The predictors  
762 were trained and evaluated on DMS data either provided by the DeMaSk study or curated by our own. The  
763 “DeMaSk data & code” result is similar to the published result. For the “Our data & DeMaSk code” result, we  
764 used our own data and published code which shows a median performance around 0.35. This is probably because



765 many more DMS results are included in our data. The similarity of results achieved using “Our data & code”  
766 demonstrates the correctness of our re-implementation.

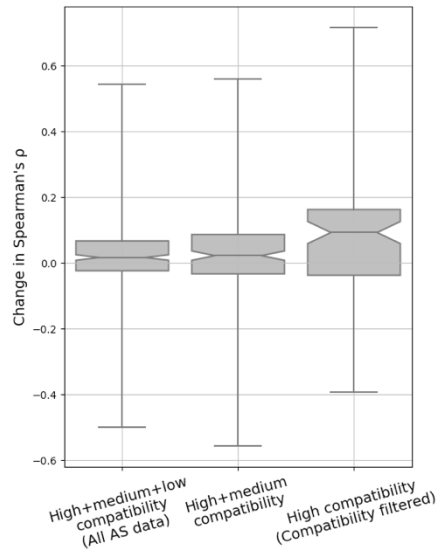
767



768

769 **Fig S4. Performance comparison between predictors using AS data or not.** The Spearman's  $\rho$  between  
770 experiment DMS scores and predicted scores for each DMS and AS data pair are shown as box plots. Different  
771 approaches to filtering/matching the data are shown on the x-axis: “All AS data” used all available data;  
772 “Compatibility filtered” used only data of high assay compatibility; “Correlation matched” used only data with  
773 the highest regularised correlation for each DMS dataset. The figure does not include data without available  
774 (filtered/matched) AS scores. This means that the different results are not directly comparable since they are  
775 visualized on different subsets of DMS/AS data pairs (for example, “All AS data” contains all DMS/AS data pairs,  
776 but “Compatibility filtered” contains only data pairs of high assay compatibility). Control results are shown as  
777 green boxes for predicting without AS data as a feature. The underlying  $\rho$  for each data pair in the control results  
778 is the same, but the boxes are shifted due to data filtering/matching.

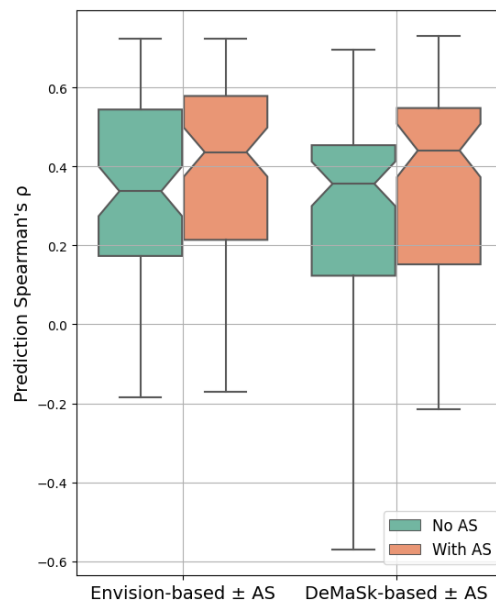
779



780

781 **Fig S5. The performance of variant impact prediction for using data of different assay compatibility levels.**

782 The change of prediction Spearman's  $\rho$  for each DMS and AS data pair is shown as box plots. A higher value  
 783 represents higher prediction accuracy achieved for using AS data. Different data filtering methods are shown on  
 784 the x-axis.

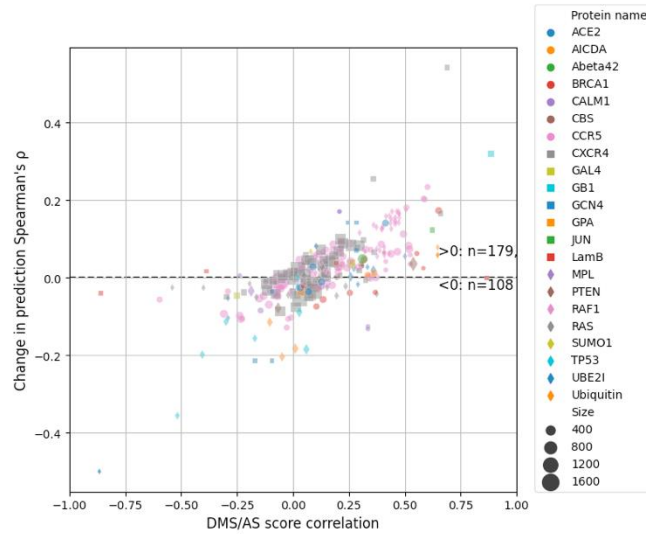


785

786 **Fig S6. Prediction performance is improved while incorporating high compatibility AS data into the**

787 **Envision model.** The Spearman's  $\rho$  between experiment DMS scores and predicted scores for each high  
 788 compatible DMS/AS assay pair are shown as box plots. The x-axis shows the predictor used, either Envision or  
 789 DeMaSk. Control results are shown as green boxes for predicting without AS data as a feature.

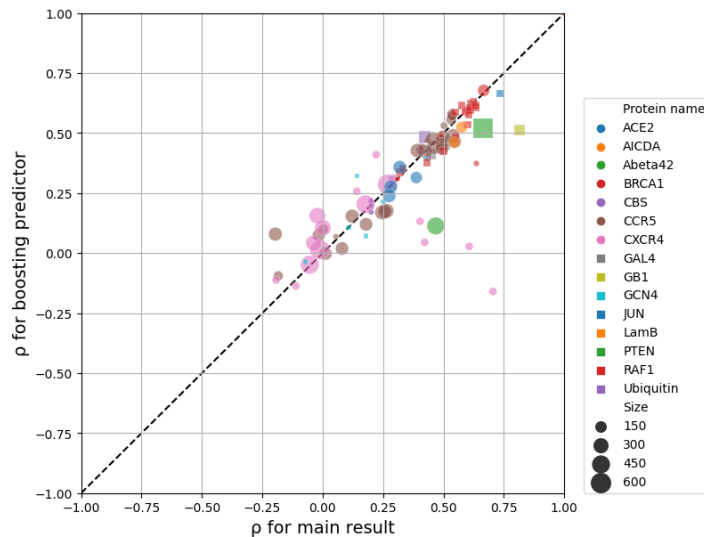
790



791

792 **Fig S7. Prediction performance change for using all AS data.** Each dot represents a DMS/AS data pair. The  
 793 vertical axis shows the change of prediction  $\rho$  by using AS data (larger means higher performance achieved by  
 794 using AS data). The horizontal axis shows the DMS/AS score correlation for *all* variants on the matched residues  
 795 rather than just alanine substitutions. The colours and shapes of the dots correspond to the target protein, and size  
 796 indicates the number of variants in each data pair.

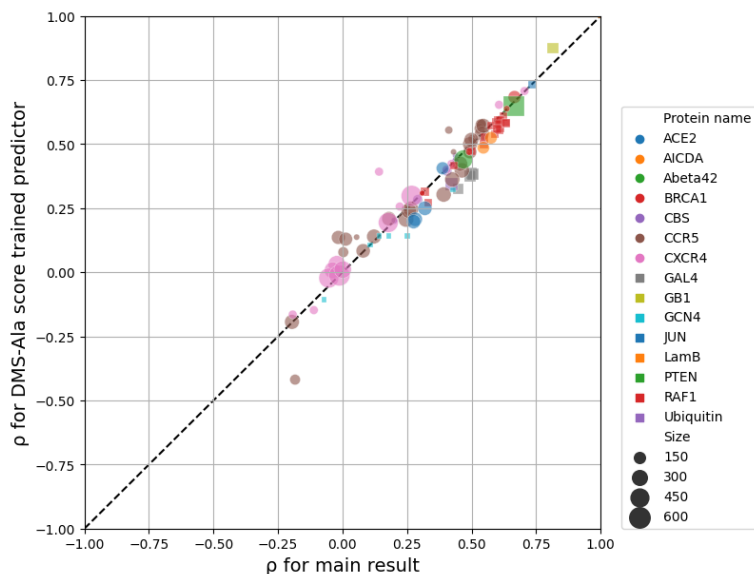
797



798

799 **Fig S8. Boosting setup shows similar performance as the main result.** Each dot represents a filtered DMS/AS  
 800 data pair of high assay compatibility. The vertical and horizontal axes show the prediction Spearman's  $\rho$  for either  
 801 modelled with boosting or the one-step (main result) setup. The colours and shapes of the dots correspond to the  
 802 target protein, and size indicates the number of variants in each data pair.

803

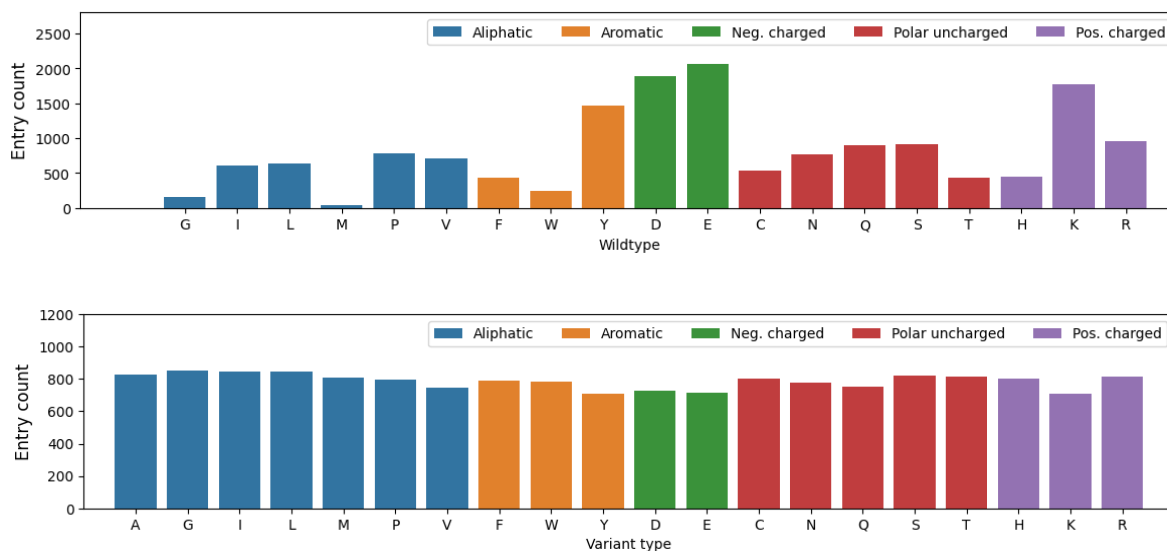


804

805 **Fig S9. Training with DMS scores of alanine substitutions shows similar performance as the main result.**

806 The vertical and horizontal axes show the prediction Spearman's  $\rho$  for predictors either trained with DMS score  
 807 of alanine substitutions (DMS-Ala) or AS data of high assay compatibility (main result), yet all evaluated on high  
 808 compatibility AS data. The colours and shapes of the dots correspond to the target protein, and size indicates the  
 809 number of variants in each data pair.

810



811

812

813 **Fig S10. Count of variant entries for each wild-type or variant amino acid of high assay compatibility data.**

814 (Neg.: negatively, Pos.: positively)

815

816 **Table S1. Amount of data with AS scores available**

<b>Data composition</b>	<b>Protein</b>	<b>DMS dataset</b>	<b>AS dataset<sup>1</sup></b>	<b>Variant entries<sup>2</sup></b>
All AS	22	54	146	70446
Compatibility filtered	15	35	60	15739
High+medium assay compatibility	21	51	105	28380
Correlation matched	22	54	32	7940

817 1. This column shows how many unique AS datasets are included.

818 2. Include duplicated variants caused by multiple experiments targeting the same protein variant.

819

## 820 **Supplementary information**

### 821 **Applying AS data to Envision method**

822 We re-implemented a predictor based on Envision [15] to incorporate AS data. Features used  
823 in Envision were downloaded from its online toolkit. All Envision features are used for  
824 modelling except for substitution type (wt\_mut) which has low importance according to the  
825 published result and our pilot studies yet is computationally expensive in our setup. Protein  
826 data were excluded if their features were not available online. DMS and AS data pairs with  
827 high assay compatibility were used for modelling. Missing feature values were imputed by the  
828 mean values for numerical features or the most frequent values for categorical features.  
829 Categorical features are encoded with the one-hot encoder. We used  
830 `sklearn.ensemble.GradientBoostingRegressor` from scikit-learn package [129]  
831 to build the predictor, and hyperparameters were tuned by Bayesian Optimization [130] with  
832 Group K-Fold (protein-30-fold) cross-validation. The training and evaluation process were  
833 similar to that previously described. For comparison, we repeated the DeMaSk-based analysis  
834 on the same subset of data.

835

### 836 **Boosting with AS data**

837 To deal with the sparsity of AS data, we tested a variant impact predictor based on boosting. A  
838 first linear regression predictor was trained with all training DMS data using the three DeMaSk  
839 features without AS data, which was the same as the control predictor mentioned previously.  
840 We then calculated the prediction error by subtracting the predicted scores from DMS scores,  
841 and a second linear regression predictor was trained to predict the error. The second predictor  
842 was trained only on DMS/AS data of high assay compatibility and used both protein features  
843 and the encoded AS scores. The final prediction result was the sum of the outputs from these  
844 two predictors.

845

### 846 **Replacing AS data with DMS scores of alanine substitutions**

847 We investigated another potential approach to overcome the sparsity of AS data by replacing  
848 the AS feature with the DMS scores of alanine substitutions (DMS-Ala). For all DMS datasets  
849 we collected, their AS feature values, regardless of availability, were replaced by the DMS-  
850 Ala scores on the same residue. Missing scores were imputed by the mean value of all DMS-  
851 Ala scores. A regression model was trained and evaluated as previously described, using the  
852 three DeMaSk features as well as the DMS-Ala scores. The AS data of high assay compatibility  
853 are still used for the testing process.

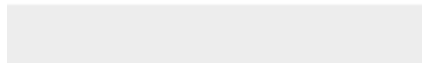
854



Click here to access/download

**Supplementary Material**

Supplementary\_Table\_1\_Supplementary Material.xlsx

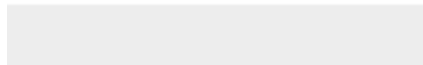




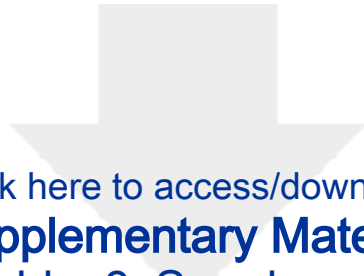
Click here to access/download

**Supplementary Material**

[Supplementary\\_Table\\_2\\_Supplementary Material.csv](#)







Click here to access/download

**Supplementary Material**

Supplementary\_Table\_3\_Supplementary Material.csv





The Walter and Eliza Hall Institute of Medical Research  
ABN 12 004 251 423  
1G Royal Parade Parkville Victoria 3052 Australia  
T +61 3 9345 2555 F +61 3 9347 0852  
[www.wehi.edu.au](http://www.wehi.edu.au)

Dr Scott Edmunds  
Editor-in-Chief  
Gigascience

Dear Dr Edmunds,

Please find our enclosed manuscript entitled “**Integrating deep mutational scanning and low-throughput mutagenesis data to predict the impact of amino acid variants**” for your consideration for publication in *Gigascience*.

The key contributions of our work are:

- We developed the first predictor of protein variant impact integrating high-throughput and low-throughput mutagenesis data, in our case, deep mutational scanning and alanine scan data.
- We demonstrate that integrative variant impact predictors improve model performance only when the high and low throughput data are generated by related assay types.

In this work, we collected high-throughput deep mutational scanning (DMS) data from an online database, with 370,000 protein variants and low throughput alanine scanning data of matched proteins from published papers. We defined a decision tree to classify low- and high-throughput assays to distinct levels of similarity across multiple categories, which we call assay compatibility. We then explored models of variant impact trained on these data. Our results showed the connection between experiment assay compatibility and the predictor’s performance built from these data.

This is an original research article, and we have no conflicts of interest to disclose. All authors have participated in the preparation of this manuscript and approved the submission of it. We confirm that this work has not been published nor is currently under consideration for publication elsewhere.

Thank you for your consideration of this manuscript.

Yours sincerely,



Mr Yunfan Fu



Prof Anthony T. Papenfuss



Dr Alan F. Rubin